Dual-Stage-Light-Guided Tumor Inhibition by Mitochondria-Targeted Photodynamic Therapy

*Kai Han, Qi Lei, Shi-Bo Wang, Jing-Jing Hu, Wen-Xiu Qiu, Jing-Yi Zhu, Wei-Na Yin, Xu Luo, and Xian-Zheng Zhang**

In this paper, a self-delivery system PpIX-PEG-$(KLAKLAK)_2$ (designated as PPK) is fabricated to realize mitochondria-targeted photodynamic tumor therapy. It is found that the PPK self-delivery system exhibited high drug loading efficacy as well as novel capacity in generation of intracellular reactive oxygen species (ROS). This study also indicated that the photochemical internalization effect of the photosensitizer protoporphyrin IX (PpIX) under a short time light irradiation improved the cellular internalization of PPK. On the contrary, PPK could target to the subcellular organelle mitochondria due to the presence of proapoptosis $(KLAKLAK)_2$ peptide. Importantly, the in situ generation of ROS in mitochondria enhanced the photodynamic therapy efficacy under another long time irradiation, leading to significant cell death with decreased mitochondrial membrane potential. Besides, relative high tumor accumulation, minimal systemic cytotoxicity and efficacious long-term tumor inhibition in vivo are also confirmed by using a murine model. All these results demonstrated the self-delivery system PPK with a dual-stage light irradiation strategy is a promising nanoplatform for tumor treatment.

1. Introduction

Fabrication of ingenious drug delivery vehicles has garnered considerable research attention during the last decade.[1–4] These vehicles were proposed to enhance therapeutic efficacy of drugs while reducing undesired side effects. However, most of these vehicles suffered from inherent restriction in low drug loading efficacy (typically less than 10%).[5,6] Consequently, high dosages of drug-loaded vehicles were always demanded to achieve satisfactory therapeutic index, resulting in severe systemic toxicity due to the poor metabolism and elimination of the vehicles.[7,8] To address this challenge, a new concept of self-delivery system has been proposed very recently.[9,10] No additional vehicles are required and high drug loading capacity can be achieved with ease in the self-delivery systems. For example, Yan and co-workers fabricated an amphiphilic biodegradable drug–drug self-delivery system for effective antitumor therapy.[11] Cui and co-workers developed a self-delivery system with the drug loading content up to 38%.[12] However, most current self-delivery systems suffered from the barrier of transforming inactive drugs to active ones rapidly and timely,[13,14] which is critical important for efficient ablation of tumor cells. The use of hydrolysable linkage such as ester bond in these self-delivery systems may arouse the concerns in biostability during blood circulation. In addition, various therapeutical compounds are always mechanically cocktail in self-delivery systems, resulting in only additive effect or weak synergistic effect.

Photosensitizer (PS)-based phototherapy as a safe and noninvasive treatment provides a new opportunity in the development of self-delivery systems. Different from traditional chemotherapeutic drugs, which initiated cell apoptosis via embedding into DNA,[15,16] antitumor effect of PS is mainly driven by the generation of reactive oxygen species (ROS) under light irradiation.[17] Therefore, the effect of phototherapy can be precisely tuned via regulating the light irradiation condition, such as time and intensity of light irradiation.[18] More interestingly, it has been well documented that PS can improve the cellular delivery of bioactive substances under a short time light irradiation, which is known as "photochemical internalization" (PCI) since the ROS-induced lipid peroxidation can improve the membrane permeability.[19] Meanwhile, longer photoperiod can kill the tumor cells via photodynamic therapy (PDT).[20] Unfortunately, ROS have a short half-life (<40 ns) and can only act to the close site of generation (<20 nm), which is much less than cell dimensions.[21] Obviously, transporting the PS to the subcellular organelle for in situ generation of ROS will be promising for improved therapeutic efficacy.

In this paper, we report a simple, but effective self-delivery system that can target to the subcellular organelle mitochondria for in situ photodynamic therapy. Here, mitochondrion is chosen as the therapeutic target due to the fact

K. Han, Q. Lei, S.-B. Wang, J.-J. Hu, W.-X. Qiu, J.-Y. Zhu, W.-N. Yin, X. Luo, Prof. X.-Z. Zhang
Key Laboratory of Biomedical Polymers of Ministry of Education and Department of Chemistry
Wuhan University
Wuhan 430072, P.R. China
E-mail: xz-zhang@whu.edu.cn
Prof. X.-Z. Zhang
The Institute for Advanced Studies
Wuhan University
Wuhan 430072, P.R. China
Prof. X.-Z. Zhang
Hubei Provincial Cooperative Innovation Center of Industrial Fermentation
Wuhan 430068, P.R. China

DOI: 10.1002/adfm.201500590

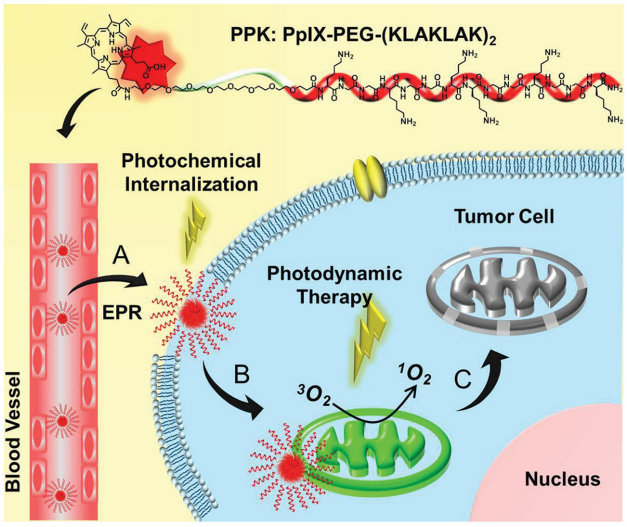

Scheme 1. Chemical structure of PPK and schematic diagram of the mitochondria-targeted self-delivering process: A) passive target to tumor cells and PCI effect enhanced cellular internalization of PPK under a short time light irradiation; B) mitochondrial targeting mediated by $(KLAKLAK)_2$; C) ROS formation, mitochondrial destruction, and cell death mediated by the synergistic effect between $(KLAKLAK)_2$ and PpIX under a long time light irradiation.

that mitochondrion is widely distributed in cytoplasm and bioactive substances can be transported to mitochondrion without hurdles such as karyotheca. On the contrary, mitochondrion as the energy center of cells manipulated many metabolic activities and mitochondrion-based chemotherapy may benefit in overcoming multidrug resistance.[22] As shown in **Scheme 1**, this self-delivery system is comprised of a photosensitizer protoporphyrin IX (PpIX) and a mitochondria-targeted amphipathic biodrug $(KLAKLAK)_2$ peptide with a short PEG linker. As a proapoptosis peptide, $(KLAKLAK)_2$ can destroy mitochondria and initiate the tumor cell apoptosis process. However, eukaryotic cell membrane is the nature barrier for transportation of $(KLAKLAK)_2$ peptide. It was envisioned that PCI effect under a short time light irradiation mentioned above could overcome this drawback. Meanwhile, the capability in mitochondria-targeting of $(KLAKLAK)_2$ peptide might enhance the photodynamic therapeutic efficacy under a long time light irradiation. Here, a dual-stage light irradiation strategy was proposed to improve the cellular internalization as well as tumor inhibition. The synergistic effect for tumor inhibition between PpIX and $(KLAKLAK)_2$ was also investigated both in vitro and in vivo.

2. Results and Discussion

2.1. Synthesis and Characterization of PPK

Since the bioactivity of PS was restricted severely by its strong hydrophobicity, in this study, conjugation of proapoptosis peptide $(KLAKLAK)_2$ to PpIX with a PEG linker was employed to improve the solubility of PpIX. The molecular weights of PPK and $(KLAKLAK)_2$ were determined by electrospray ionization mass spectrometry (ESI-MS, **Table 1**). The improved water solubility of PpIX was validated by the UV spectrum. As shown in **Figure 1**A, different from PpIX, a sharp Soret band around 400 nm was observed, demonstrating that negligible π–π stacking induced aggregation existed.[23] Meanwhile, enhanced water-solubility could significantly facilitate the generation of singlet oxygen ($^1O_2$). As shown in Figure 1B, optical intensity of p-nitroso-*N*,*N*′-dimethylaniline (RNO, $^1O_2$ sensor) at 440 nm decreased rapidly when PPK received light irradiation, suggesting the rapid generation of plenty of $^1O_2$ as well as oxidation of RNO. In contrast, due to the self-quenching of free PpIX, undetectable optical intensity change of RNO was observed, indicating the disappointing capability of PpIX in formation of $^1O_2$ in aqueous medium. Besides, dynamic light scattering (DLS) and transmission electron microscope (TEM) studies revealed that amphiphilic PPK could self-assemble into well-dispersed, spherical nanoparticles with a hydrodynamic size of 91.0 nm (Figure 1C,D). Note that the particle size measured by DLS was nearly threefolds to that observed by TEM, since TEM sample was observed in vacuum state and PPK would shrink.[6] The nanoparticles in the sub-100 nm range always had great potential in preferentially accumulating in tumor tissue.[24] In addition, although PPK could self-assemble to form nanoparticles, very limited self-quenching was observed when the concentration of PPK was below 200 μg mL^{-1} (Figure S1A,B, Supporting Information), since the nanoparticles were not compact enough.

Table 1. Peptide sequences and the corresponding molecular weights.

Peptide sequence	Molecular weight[a)]	$[M + 2H]^{2+}$ [b)]
$(KLAKLAK)_2$	1522.08	762.2
PpIX–PEG–$(KLAKLAK)_2$	2489.58	1246.0

[a)]Theoretical molecular weight; [b)]$[M + 2H]^{2+}$ was found in ESI-MS spectrum.

2.2. Intracellular ROS Generation Observed by Confocal Laser Scanning Microscopy (CLSM)

Having confirmed the novel ROS generation property of PPK in aqueous medium, we proceeded to test the intracellular ROS generation in HeLa cells via confocal laser scanning microscopy (CLSM). For comparison, blank cells and cells treated with $(KLAKLAK)_2$ or PpIX were used as negative controls using 2′,7′-dichlorofluorescin diacetate (DCFH-DA) as the ROS sensor. It was known that DCFH-DA has nonfluorescence. Once exposed to ROS, DCFH-DA can be oxidized to 2′,7′-dichlorofluorescin (DCF) with green fluorescence. **Figure 2**A1,B1 revealed that weak green fluorescence was found in blank cells and $(KLAKLAK)_2$-treated cells, respectively. In contrast, remarkable green fluorescence was observed in the PPK group (Figure 2D1), verifying the formation of intracellular ROS under light irradiation. Interestingly, it was found that the green fluorescence in cytoplasm was significantly higher than that in cell nucleus. Meanwhile, the green fluorescence in cytoplasm was spotty (Figure 2D1) due to the mitochondria-targeting effect of $(KLAKLAK)_2$.[25] In situ generation of ROS in scattering distributed mitochondria led to stronger green fluorescence in cytoplasm. Additionally, free PpIX also

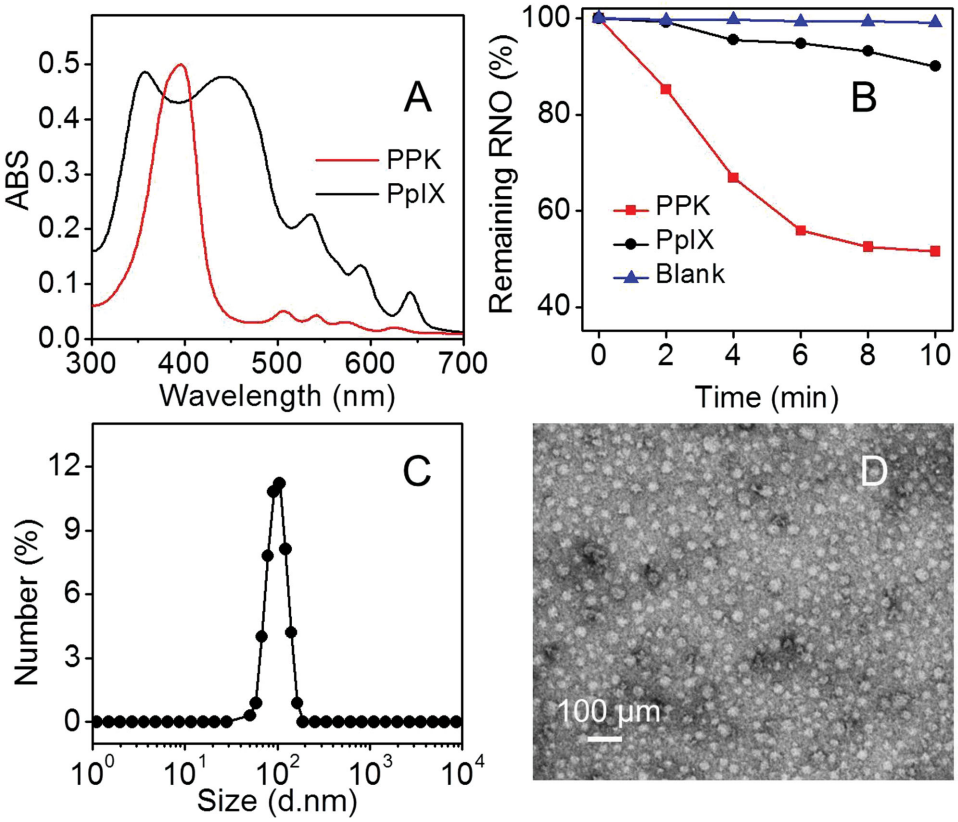

Figure 1. A) UV–vis spectrum of PPK in DI water and PpIX in DMSO/H_2O mixtures (v:v = 5:95). B) Singlet oxygen generation was measured using RNO as a sensor according to irradiation time, using RNO alone with light irradiation as the blank control. Hydrodynamic size C) and TEM image D) of PPK in DI water. The concentration of PPK was 40 μg mL^{-1}.

triggered certain amount of ROS generation (Figure 2C1). It was noticed that the quantity difference in ROS generation between PPK and PpIX determined by CLSM was smaller than that determined by fluorescence spectrum (Figure 1B), owing to the higher sensitivity of DCFH-DA to ROS.

2.3. Synergetic Therapeutic Efficacy and PCI-Induced Internalization

Recent studies suggested that the PCI effect of photosensitizer could enhance the cellular uptake of bioactive substances.[26,27] Based on this property, we anticipated that a dual-stage light irradiation strategy integrating PCI with PDT may optimize the tumor inhibition efficacy. In order to confirm this speculation, MTT assay against HeLa cells was conducted to evaluate in vitro cytotoxicity of PPK under a dual-stage light irradiation, i.e., a short time light irradiation during cellular internalization followed by another long time light irradiation after cellular internalization. Cytotoxicity of PPK under 24-min light irradiation was determined as the control. It was found that once the PPK received 24-min irradiation, significant cytotoxicity was observed and the IC_{50} was 40 mg L^{-1} (**Figure 3**A). The cytotoxicity was further enhanced when the dual-stage light irradiation (6 + 18 min) was employed. It was inferred that photosensitizer under a short time light irradiation disintegrated the cellular membrane via ROS-mediated lipid peroxidation.[28] As a result, the improved membrane permeability led to the enhanced cellular uptake of PPK as well as cytotoxicity. In addition, PPK exhibited slight dark cytotoxicity (Figure 3B), while 6-min light irradiation increased the cytotoxicity insignificantly, suggesting that unlike PDT, PCI did not influence the cell viability dramatically.

Considering that both PpIX and $(KLAKLAK)_2$ could inhibit tumor growth, the synergetic efficacy of PpIX and $(KLAKLAK)_2$ in PPK was evaluated. As shown in Figure 3C, the cytotoxicity increased slowly with increasing amount of PpIX owing to the poor bioavailability of free PpIX as well as the low efficacy in ROS generation. Meanwhile, proapoptosis $(KLAKLAK)_2$ peptide also performed unapparent cytotoxicity and above 85% cells were still survived even when the concentration of peptide was up to 175 mg L^{-1} (Figure 3D). This was attributed to the eukaryotic plasma membrane barrier to $(KLAKLAK)_2$. It has been well documented that although $(KLAKLAK)_2$ possessed the ability to destroy the mitochondria, it could not pass the eukaryotic plasma membrane, leading to the low cellular uptake of $(KLAKLAK)_2$ as well as disappointing cytotoxicity.[29,30] The combination index[31] with a dual-stage light irradiation strategy was far below 1 (data not shown), demonstrating the novel synergy between PpIX and $(KLAKLAK)_2$ in PPK. This novel synergistic efficacy was attributed to following facts: modification of hydrophobic PpIX with cationic proapoptosis $(KLAKLAK)_2$ peptide

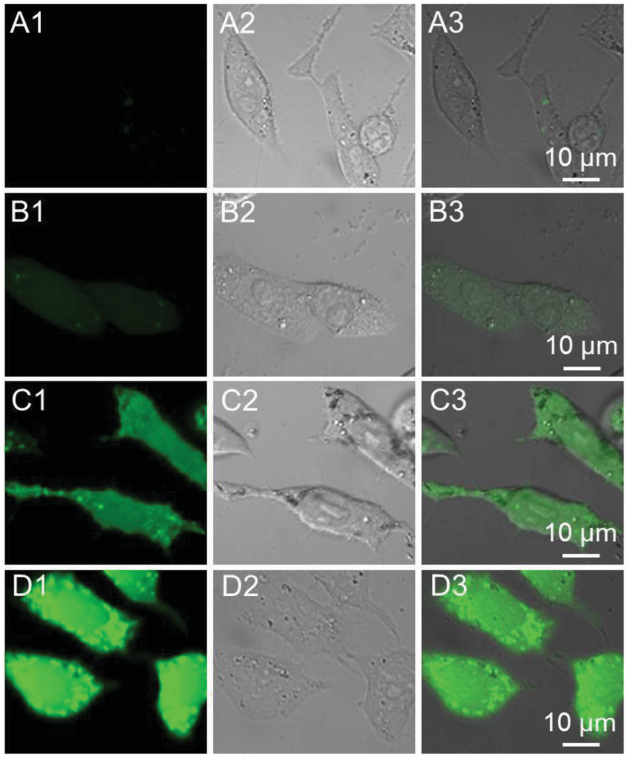

Figure 2. The generation of intracellular ROS mediated by various samples: A1–A3) blank control; B1–B3) $(KLAKLAK)_2$; C1–C3) PpIX with light irradiation; D1–D3) PPK with light irradiation. A1–D1: DCF fluorescence (green) depicted intracellular ROS; A2–D2: bright fields. A3–D3: overlay images.

greatly enhanced the bioactivity of PpIX. Moreover, the PCI of PpIX under a short light irradiation increased the cellular internalization of PPK. Subsequently, proapoptosis $(KLAKLAK)_2$ peptide could not only disrupt mitochondrial membrane, but also guide the PPK to the mitochondria. Consequently, the in situ generation of ROS in the mitochondria under a long time light irradiation dramatically decreased the integrity of mitochondrial membrane, leading to significantly improved photodynamic therapy.

Furthermore, CLSM and flow cytometric analysis were employed to visualize PCI-enhanced cellular internalization of PPK. As show in **Figure 4**A, a larger area of red fluorescence was observed when the cells received 6-min light irradiation than that without light irradiation, which substantially indicated that the short light irradiation could enhance the cellular uptake of PPK. Quantitative results via flow cytometric analysis showed that the mean fluorescence intensity (MFI) value under 6-min light irradiation was nearly two folds to that without light irradiation (Figure 4C,D). All these results were consistent with the cytotoxicity studies. Besides, the mitochondrial targeting ability of PPK was also determined by CLSM. The mitochondria were stained with a green dye, MitoTracker Green. As shown in Figure 4A3, the majority of red fluorescence was overlapped well with green fluorescence, suggesting the PPK could target to mitochondria efficiently. Pearson's correlation coefficient ($p = 0.47$) [32] and fluorescence-intensity-profile analysis [33] also confirmed it (Figure S2B, Supporting Information). Since mitochondrial membrane potential was extremely low, cationic $(KLAKLAK)_2$ could preferentially interact with mitochondria, which led to the specific accumulation of PPK in mitochondria.

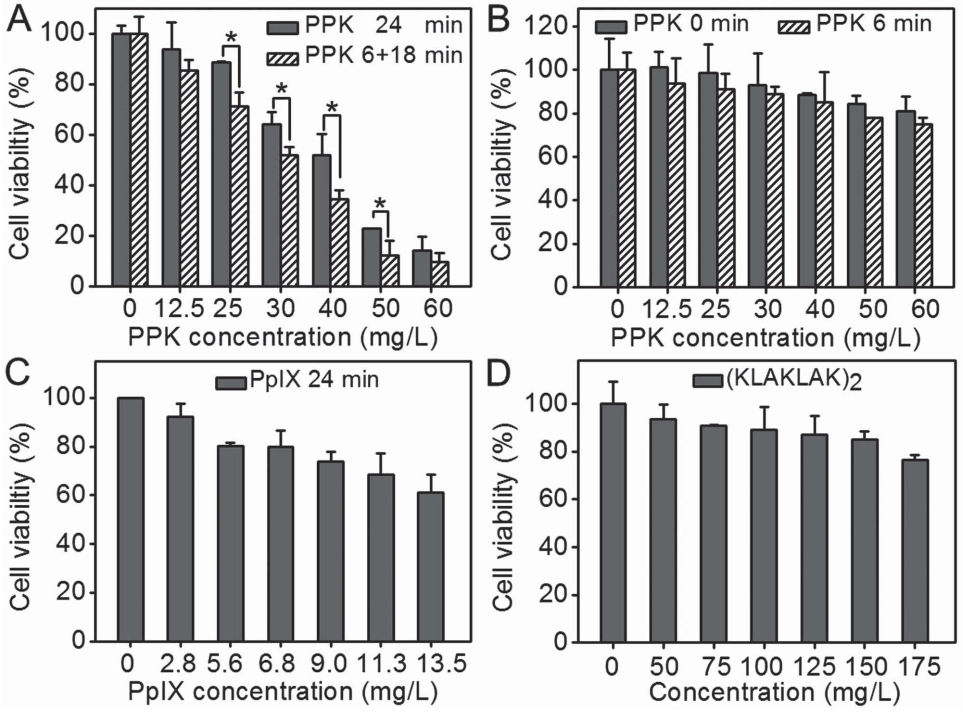

Figure 3. In vitro cell viability against HeLa cells: A) PPK under 24-min light irradiation and 6+18 min light irradiation, respectively; B) PPK without light irradiation and under 6-min light irradiation were used as controls; C) PpIX under 24-min light irradiation; D) $(KLAKLAK)_2$. $*p < 0.01$, when the group was compared with cells treated with PPK with 24-min light irradiation as determined by a Student's t-test.

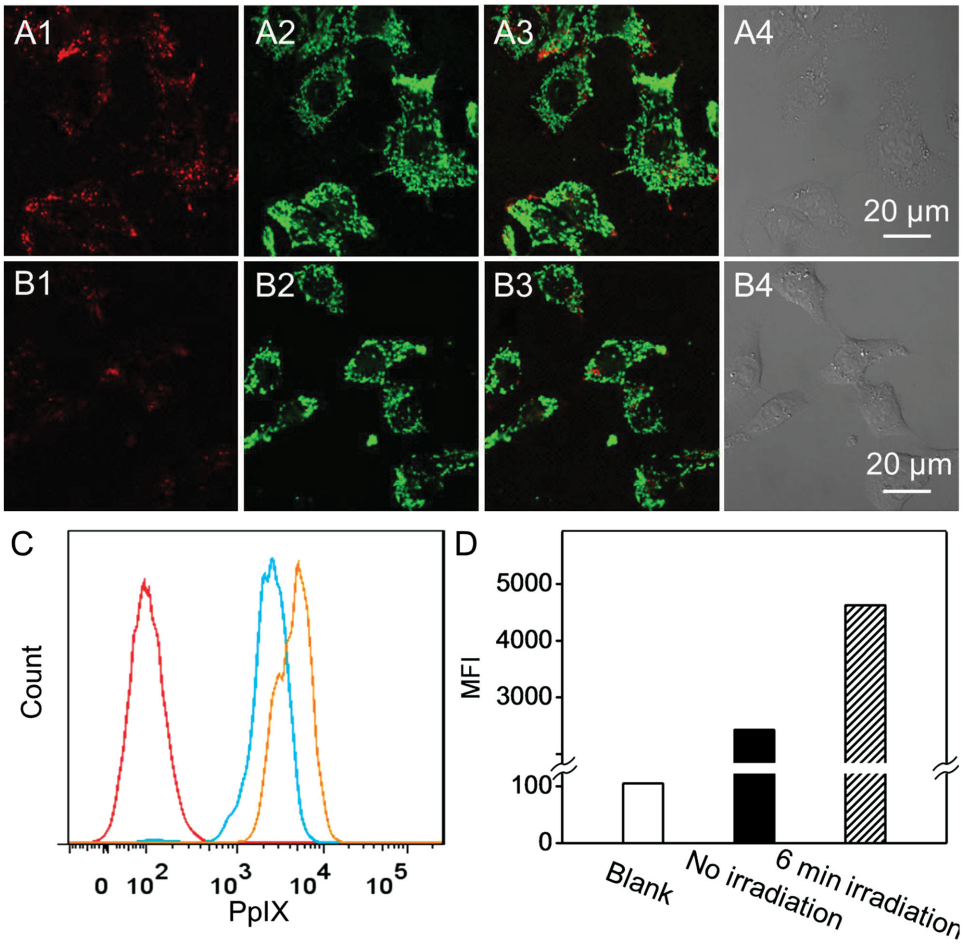

Figure 4. Cellular uptake and mitochondrial targeting effect of PPK in HeLa cells: A1–A4) PPK under 6-min light irradiation during internalization; B1–B4) PPK without light irradiation during internalization. Green channel: MitoTracker Green. Red channel: PpIX. A3 and B3: the emerged images of green and red signals. A4 and B4: the bright fields. C–D) Flow cytometric analysis of PPK in HeLa cells under 6-min light irradiation during internalization (orange line), without light irradiation during internalization (blue line) and blank group (red line).

Besides, the early apoptosis behaviors mediated by various samples were observed in situ via CLSM using Annexin V-FITC as the sensor. As shown in **Figure 5**, cells treated with $(KLAKLAK)_2$ almost had no green fluorescence, which was similar to that in blank cells, indicating the negligible cytotoxicity of $(KLAKLAK)_2$. Meanwhile, the green fluorescence increased with the following order: PpIX under 24-min light irradiation < PPK under 24-min light irradiation < PPK under dual-stage light irradiation.

2.4. Mitochondrial Membrane Potential Measurement

In order to get direct insight to the toxic mechanism of PPK, the mitochondrial membrane potential was determined using JC-1 dye as the sensor.[34] It has been well recognized that the decrease of mitochondrial membrane potential is a crucial indicator to assess the dysfunction of mitochondria. JC-1 trends to aggregate in cells with high mitochondrial membrane potential, but become monomeric in cells with low mitochondrial membrane potential. Meanwhile, the JC-1 dye suffers a reversible change in fluorescence emission that aggregated JC-1 fluoresces red and monomeric JC-1 fluoresces green. Therefore, the red/green fluorescence ratio can be used to assess the status of mitochondria as well as cells to some extent.

The representative results of JC-1 assays against HeLa cells were performed in **Figure 6**. Obviously, with increasing light irradiation time, the green fluorescence increased while the red fluorescence decreased, indicating that the generation of ROS could damage mitochondria and lead to the loss of the mitochondrial membrane potential. The flow cytometric analysis also confirmed that the percentage of positive green fluorescence (in the triangle) increased with the delay of light irradiation (Figure 6A5–D5). It was noteworthy that the red fluorescence was very weak in the majority of HeLa cells when the cells received only 18-min light irradiation. Clearly, PPK could damage the cells at a relative low dose of light irradiation. This finding was attributed to mitochondrial targeting effect of $(KLAKLAK)_2$. Mitochondria as the energy houses of cells played an important role in energy metabolism of various biological processes, including cell apoptosis. Although PpIX could produce ROS under light irradiation, the short lifetime and limited

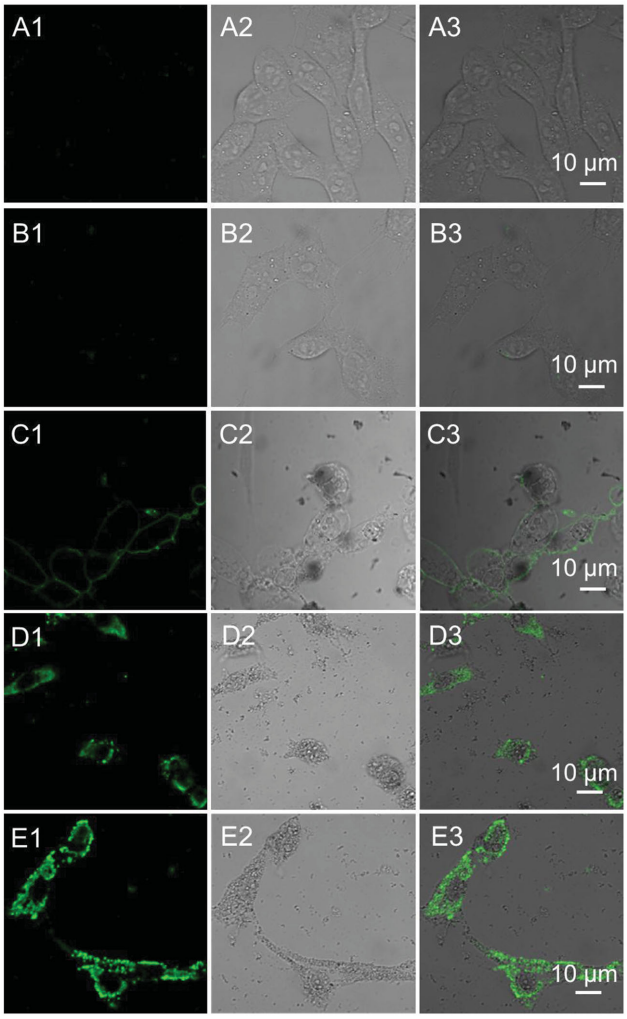

Figure 5. Early apoptosis of A1–A3) blank cells, B1–B3) $(KLAKLAK)_2$, C1–C3) PpIX with 24-min light irradiation, D1–D3) PPK with 24-min light irradiation, E1–E3) PPK with 6 + 18 min light irradiation against HeLa cells were observed by CLSM. A1–E1: Annexin V-FITC stain (green) depicted apoptotic cells; A2–E2: bright fields. A3–E3: overlay images.

action region of ROS restricted the therapeutic efficacy. This targeting effect of $(KLAKLAK)_2$ led to in situ generation of ROS in mitochondria, resulting in enhanced destructive power of ROS to cells.

2.5. Long-Term Synergetic Antitumor Study In Vivo via Subcutaneous Injection

To further estimate the in vivo synergetic therapeutic efficacy between PpIX and $(KLAKLAK)_2$ under a dual-stage light irradiation in the self-delivery system, H22-bearing mouse animal mode with subcutaneous injection was used for long-term antitumor study. Here, subcutaneous injection was chosen with the following reasons: free PpIX as an indispensable control was not suitable for intravenous injection, since it would induce blood blockage and mice died quickly during intravenous injection due to the poor solubility in physiological conditions (data not shown). On the contrary, subcutaneous injection could increase drug concentration at the tumor site and ensure the controllable dosages of various samples in the tumor tissue regardless of pharmacokinetic discrepancy among different drugs. Before that, intratumoral fluorescence distributions of PpIX and PPK were determined in **Figure 7**A. Due to the self-quenching of free PpIX, fluorescence was nearly undetectable. And this result was also confirmed by the fluorescence spectrum of PpIX (Figure S1C, Supporting Information). In marked contrast, strong fluorescence was observed during 1 day postinjection. The fluorescence was still strong even at the 4th day. This stable fluorescence of PPK in the tumor tissue was favorable for long-term dual-stage-light-guided photodynamic therapy. When the mice were killed at the 10th day, the organs, muscle and tumor tissue were also peeled and imaged (Figure 7B). It was found that the fluorescence of PPK in tumor was significantly higher than that in muscle, heart, liver, spleen, lung, and kidney. Similar finding was also observed in PpIX-treated mice. These results confirmed that therapeutic agents could efficiently stay in tumor via subcutaneous injection.

Furthermore, it was found that for the mice injected with PPK under 5+15 min light irradiation, significant inhibition of tumor growth was observed at the 5th day (Figure 7C), indicating the successful tumor suppression of PPK with a dual-stage-light strategy. For comparison, only limited therapeutic efficacy was found in the mice that were administrated with PpIX under 20-min light irradiation or $(KLAKLAK)_2$, owing to the hydrophobic nature of PpIX and poor cellular uptake of $(KLAKLAK)_2$ respectively as mentioned above. When the mice were sacrificed at the 12th day, there existed considerable difference in the tumor weights between the group treated with PPK and other groups (Figure 7E), illustrating the good synergistic efficacy of the self-delivery system in vivo. And this result was also visually evidenced by the representative tumor images in Figure 7F. Meanwhile, the relative body weight of mice treated with PBS increased gradually (Figure 7D), probably due to the increased tumor weight. In contrast, administration with PPK did not influence the body weight, suggesting negligible systemic toxicity of PPK. Furthermore, hematoxylin and eosin (H&E) staining images of the tumor tissues at the 12th day were also performed. When the mice were administrated with PPK for 5+15 min light irradiation, most tumor cells were killed (Figure 7J). On the contrary, in the case of $(KLAKLAK)_2$ (Figure 7H) or PpIX (Figure 7I), only limited tumor cells showed apoptosis/necrosis while most tumor cells were survived in the PBS group (Figure 7G). All these results demonstrated the efficiently synergistic antitumor activity in vivo of the self-delivery system.

2.6. Tumor Imaging, Biodistribution, Blood Retention Time, and Antitumor Study In Vivo via Intravenous Injection

Considering that PPK could form nanoparticles in the sub-100 nm range, and the self-delivery system achieved good mitochondria-targeted tumor inhibition both in vitro and in vivo via subcutaneous injection, the medicine translational potential of PPK in antitumor therapy was further evaluated in terms of in vivo biodistribution as well as antitumor effect after

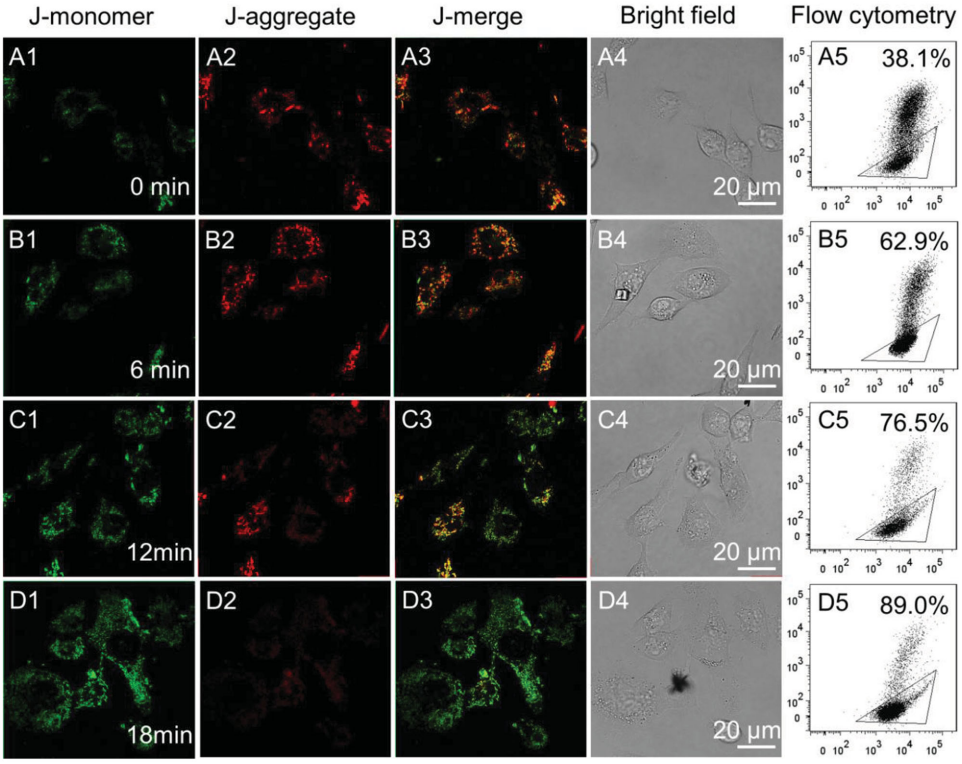

Figure 6. CLSM images and the corresponding flow cytometric analysis of mitochondrial membrane potential for HeLa cells when the cells were incubated with 40 μg mL^{-1} of PPK and then performed with different time irradiations: A1–A5) without light irradiation (the control); B1–B5) with 6-min light irradiation; C1–C5) with 12-min light irradiation; D1–D5) with 18-min light irradiation. For A5–D5, triangle separated populations with high (inside the triangle) and low membrane potential (outside the triangle). The horizontal axis was green fluorescence while the vertical axis was red fluorescence. JC-1 was used as an indicator.

intravenous injection. PpIX was not used as a negative control as mentioned above. As shown in **Figure** 8A, PPK gradually accumulated in the tumor, and strongest fluorescence was observed after 7 h. Subsequently, the fluorescence decreased due to the metabolism. Similar result was found in blood retention time study (Figure 8B). The standard curve of PPK in blood was performed in Figure S3 (Supporting Information). Cleary, PPK kept a high concentration in the bloodstream even up to 8 h. At the 24th h after intravenous injection, the H22 tumor bearing mice were sacrificed. Figure 8C presented the MFI of PPK in the tumors and other organs. Although great PPK accumulated in the liver, the amount of PPK in tumor was still comparable with that in kidney and significant higher than that in heart, spleen, lung and muscle. In all, PPK could passively target and accumulate in tumor region via enhanced permeability and retention (EPR) due to the self-assembly of PPK into nano-sized particles.

Encouraged by the efficient accumulation of PPK in tumor, the feasibility of PPK in antitumor therapy in vivo was tested via intravenous injection. PBS and $(KLAKLAK)_2$ were employed as the controls. As shown in Figure 8D, PBS and $(KLAKLAK)_2$ could not inhibit the tumor growth. In sharp contrast, PPK significantly depressed the tumor progression. The tumor volume was less than half the size in PBS group at the 10th day. This good therapeutic effect of PPK was also confirmed directly by the tumor weights (Figure 8F) and representative tumor images (Figure 8G). Meanwhile, negligible change in mice body weight was also observed (Figure 8E) when the mice were treated with PPK under irradiation, indicating the negligible systemic cytotoxicity of PPK. The satisfactory therapeutic efficacy with minimal systemic toxicity was further confirmed by standard H&E staining (Figure 8H). Compared with the results in both PBS and $(KLAKLAK)_2$ groups, no obvious physiological morphology changes were found in muscle, heart, liver, spleen, lung, and kidney when the mice were treated with PPK, indicating the low systemic toxicity. However, many tumor cells were dead in the PPK group. In our opinion, the dramatically reduced systemic toxicity was attributed to passive tumor target effect, superiority of PPK self-delivery system and optical-imaging-guided tumor phototherapy. Unlike the other chemical drugs such as cisplatin, camptothecin and doxorubicin whose toxicity was always "On", the systemic toxicity of PPK was silenced during blood circulation. Moreover, PpIX had a long emission wavelength, which was in favor of optical imaging in vivo. Once PPK accumulated in tumor via passive tumor target effect, optical-imaging guided, tumor region specific photodynamic therapy restricted the active region of ROS, leading to reduced systemic toxicity. It should be pointed out that although dramatically reduced systemic toxicity was realized in both subcutaneous injection and intravenous injection, the therapeutic efficacy via subcutaneous injection was better than that via intravenous injection.

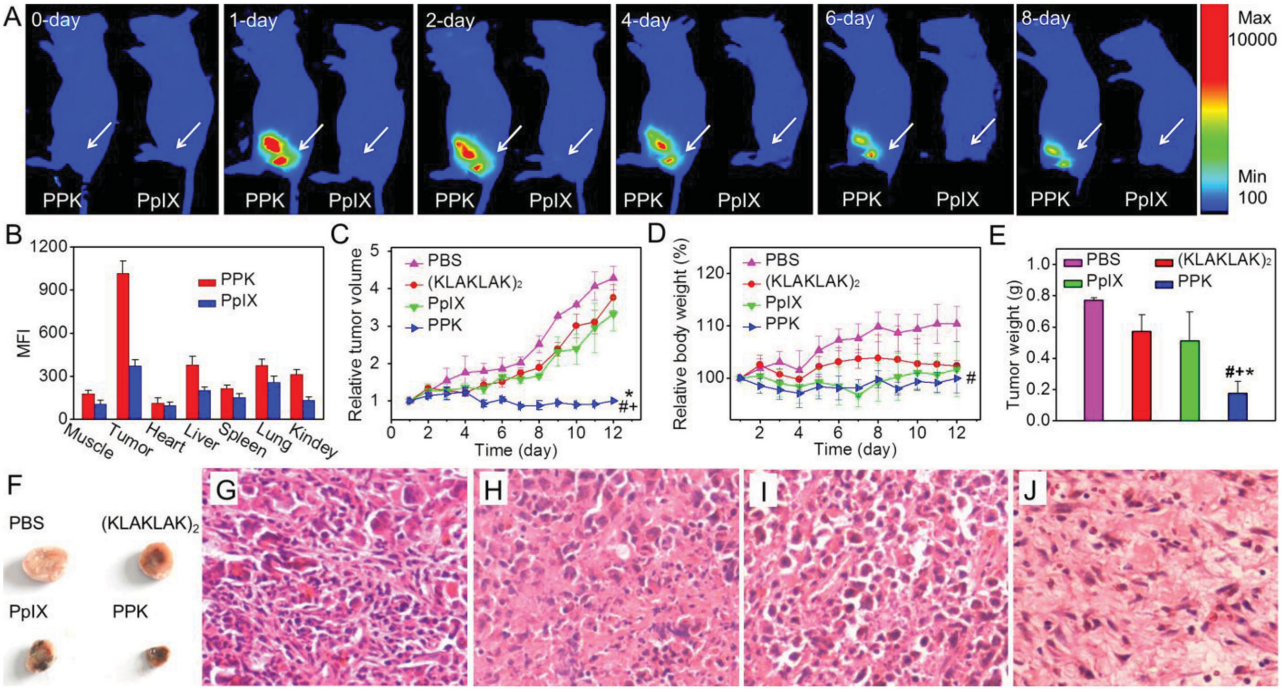

Figure 7. Tumor imagings and antitumor study in vivo via subcutaneous injection. A) Intratumoral fluorescence distributions of PpIX and PPK; B) tissue distribution of PPK and PpIX at the 10th day after subcutaneous injection; C) relative tumor volume after posttreatment; D) relative body weight when the mice were treated with different samples; E) the average tumor weight at the 12th day after posttreatment; F) representative images of the tumors at the 12th day after posttreatment. $^{\#}p < 0.05$, $^{+}p < 0.05$ and $^{*}p < 0.05$ were determined by a Student's t-test when the group was compared with the groups that treated with PBS, $(KLAKLAK)_2$ and PpIX, respectively. H&E staining images of tumor tissues which were sacrificed at the 12th day after treatment of various samples: G) PBS; H) $(KLAKLAK)_2$; I) PpIX under 20-min light irradiation; J) PPK under 5+10 min light irradiation.

3. Conclusions

In this paper, we developed a mitochondria-targeted self-delivery system PPK for dual-stage-light-guided tumor inhibition. In this self-delivery system, proapoptosis $(KLAKLAK)_2$ peptide and PS could be transported to tumor cells with a high drug loading efficacy. PCI effect under a short time light irradiation improved the cellular uptake of PPK. In turn, the mitochondria-targeting effect of proapoptosis $(KLAKLAK)_2$ peptide realized the in situ formation of ROS under a long time light irradiation in mitochondria, leading to enhanced photodynamic therapy effect. This dual-stage-light strategy in the self-delivery system ensured the efficiently synergistic tumor inhibition both in vitro and in vivo. We believe that this dual-stage-light-guided, mitochondria-targeted photodynamic therapy opens a window in the development of self-delivery system for tumor inhibition.

4. Experimental Section

Materials: Detailed material information was provided in our previous article.[35] Additionally, Fmoc-PEG_8-COOH was provided by Zhoubei Technology Co. Ltd. (Hangzhou, China). JC-1 was obtained from Qcbio Science & Technologies Co. Ltd. (China). PpIX was purchased from Aladdin-Reagent Co. Ltd. (China). MitoTracker Green was provided by Sigma-Aldrich. p-nitroso-*N*,*N*′-dimethylaniline (RNO) was obtained from TCI (Shanghai) Development Co. Ltd. 2′,7′-dichlorofluorescin diacetate (DCFH-DA) was provided by Beyotime Institute of Biotechnology (China).

Cell Culture: HeLa cells were cultured in DMEM medium in an atmosphere of 5% CO_2 at 37 °C. The medium contained 1% antibiotics (penicillin-streptomycin, 10 000 U mL^{-1}) and 10% heat-inactivated FBS.

Synthesis of Peptides: PpIX-PEG-$(KLAKLAK)_2$ and $(KLAKLAK)_2$ were synthesized as our previous report.[36] Briefly, peptide sequence was linked to Rink-NH_2 resin (0.69 mmol g^{-1}). The peptide was cleaved from resin with a cleavage cocktail of trifluoroacetic acid (TFA), DI water and triisopropylsilane in the volume ratio of 95 : 2.5 : 2.5 for 1.5 h. The final product was lyophilized. The molecular weight was determined by ESI-MS (Finnigan LCQadvantage).

Particle Size Measurement: Nano-ZS ZEN3600 (Malvern Instruments) was used to detect the particle size at 25 °C. Particle size was measured in water. The concentration of PPK was 40 μg mL^{-1}.

TEM Observation: Morphology of various samples was observed by TEM (JEM-2100 microscope). The sample was stained with 0.2% (w/v) phosphotungstic acid solution.

Singlet Oxygen Detection: The generation of $^1O_2$ was determined by following the loss of UV absorbance of disodium salt of RNO in the PPK solution.[37] Briefly, RNO (50 μL, 5×10^{-5} M) and histidine (150 μL, 6×10^{-5} M) were mixed with 760 μL distilled water, and then fresh PPK solution (40 μL, 1 mg mL^{-1}) was added. The solution was illuminated under a laser light (630 nm He-Ne laser, 40 mW cm^{-2}). The UV absorption at 440 nm (λ_{max} of RNO) was recorded every 2 min to monitor the consumption of RNO. Besides, the generation of intracellular ROS was measured via CLSM using DCFH-DA as the sensor. HeLa cells were incubated with various samples for 4 h. And then the medium was replaced. DCFH-DA was added (final concentration 1×10^{-5} M) and the cells were incubated for 20 min. 12-min light irradiation was performed subsequently (band pass: 400–700 nm, 3.3 mW cm^{-2}). The cells were repeatedly washed and then observed as soon as possible via CLSM. A 488 nm argon laser was used for excitation, while the emission was collected at 510–540 nm.

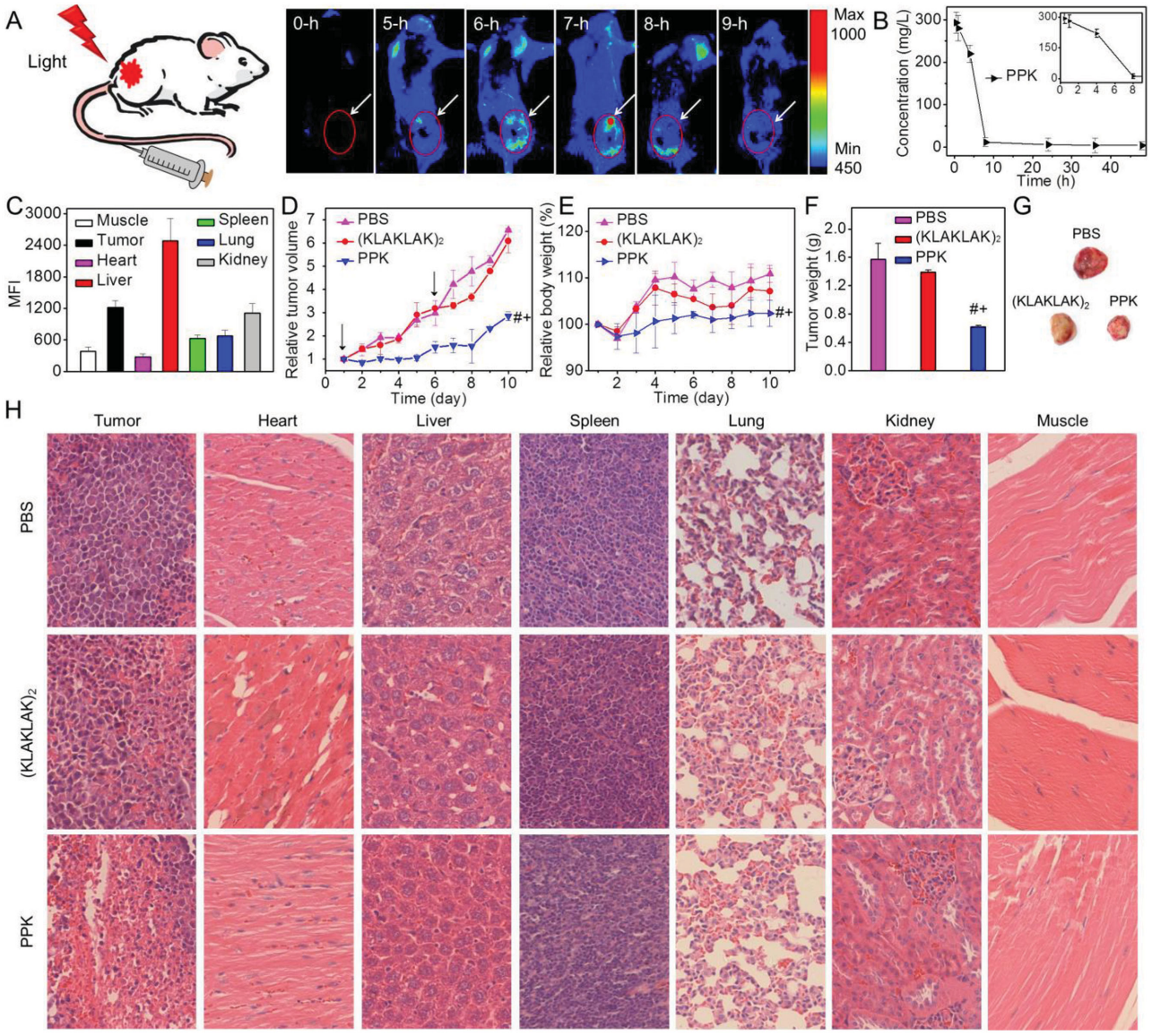

Figure 8. Biodistribution and antitumor study in vivo via intravenous injection. A) Body imaging of H22 tumor-bearing mice after intravenous injection of PPK, the white arrow pointed at tumor; B) blood retention kinetics of PPK (at 5 mg PpIX equiv. kg^{-1}) after intravenous injection; C) tissue distribution of PPK at 24 h during postinjection; D) relative tumor volume after posttreatment, the black arrow represented the first and second injection, respectively; E) relative body weight when the mice were treated with different samples; F) average tumor weight at the 10th day after posttreatment; G) representative images of the tumors after posttreatment. $^{\#}p < 0.05$ and $^{+}p < 0.05$ were determined by a Student's t-test when the group was compared with the groups that treated with PBS and $(KLAKLAK)_2$, respectively. H) H&E staining images of tumor tissues and other organs which were sacrificed at the 10th day after treatment of various samples.

Cytotoxicity Assay: The cytotoxicity of various samples in HeLa cells was determined via MTT assay. Briefly, the cells were seeded on a 96-well plate at a density of 6000 cells/well in 100 µL DMEM containing 10% FBS. After incubated for 24 h, samples with various concentrations were added to each well. 4 h later, the medium was replaced with 200 µL fresh medium and light irradiation was performed for preset time (band pass: 400–700 nm, 3.3 mW cm^{-2}). Subsequently, the cells were incubated for 48 h, 20 µL MTT (5 mg mL^{-1}) solution was added. After incubated for another 4 h, the medium was replaced with 200 µL DMSO. The OD values were measured at 570 nm. The cell viability was defined as the percentage of survival cells per total nontreated cells. Specially, the PCI-enhanced cytotoxicity was determined in a different way: when the PPK was added to 96-well plate for 1 h, 6-min light irradiation was performed. When the fresh medium was added after 4 h endocytosis, 18-min light irradiation was performed again.

Early Apoptosis Measurement: HeLa cells were seeded in a 6-well plate and allowed to attach for 1 day. Then the medium was replaced with various samples in DMEM ($(KLAKLAK)_2$ 24.5 µg mL^{-1}, PpIX 9 µg mL^{-1}, and PPK 40 µg mL^{-1}). 4 h later, the medium was replaced with FBS. PpIX group received 24-min light irradiation while PPK group received 6 + 18 min light irradiation (band pass: 400–700 nm, 3.3 mW cm^{-2}). Cells were further incubated for 6 h and then washed with PBS for once. Thereafter, cells were incubated with Annexin V-FITC in Binding Buffer for 10 min. The early apoptosis mediated by various samples were tested by CLSM (C1-Si, Nikon, Japan). The fluorescence images were observed with a filter set (E_x = 488 nm and E_m = band pass 500–550 nm) for Annexin V-FITC.

PCI-Mediated PPK Internalization and Colocalization Imaging: HeLa cells (1×10^5 cells per well) were seeded in a 6-well plate. 24 h later, the medium was replaced with 40 μg mL PPK (in 10% FBS). Cells received 6-min light irradiation (band pass: 400–700 nm and 3.3 mW cm^{-2}) after 1 h and were further incubated for 3 h. The medium was extracted and cells were washed with PBS to remove free PPK. Subsequently, the MitoTracker Green was added to stain the mitochondria for 30 min. The cells were imaged directly via CLSM after repeated washing with PBS. The fluorescence images were observed with a filter set (E_x = 488 nm, E_m = band pass 500–550 nm) for MitoTracker Green and a filter set (E_x = 409 nm and E_m = band pass 600–700 nm) for PpIX. Additionally, the PCI-mediated PPK internalization was also measured via flow cytometric analysis. After the cells received 6-min light irradiation and were further incubated for 3 h, cells were washed with PBS repeatedly. Then the cells were detached with 0.25% trypsin, harvested and washed twice with PBS. The samples were tested on Beckman Flow Cytometer (Epics XL) and the results were analyzed with Flowjo 7.6 software.

Mitochondrial Membrane Potential Determination: CLSM and flow cytometric analysis were employed to investigate the mitochondrial membrane potential in HeLa cells. For CLSM, the cells were seeded in the 6-well plate at a density of 1×10^5 cells per well. After incubated for 24 h at 37 °C, the medium was extracted and the cells were washed twice with PBS. Thereafter, 40 μg mL^{-1} PPK in 10% FBS was added. After 4 h, the medium was removed and cells were washed with PBS for three times. Then light irradiation was performed (band pass: 400–700 nm and 3.3 mW cm^{-2}) for preset time. Subsequently, the cells were incubated for 30 min. Then the mitochondria were stained with JC-1 (final concentration: 2.5 μg mL^{-1}) for 30 min. Cells were washed with PBS three times again. And the fluorescence was analyzed by CLSM (C1-Si, Nikon, Japan) equipped with a 488 nm argon laser for excitation. Light emissions were collected at 510–540 nm (green) and at 570–600 nm (red). For flow cytometery, after 40 μg mL^{-1} PPK was internalized by HeLa cells for 4 h, the cells were rinsed with PBS thoroughly. Then light irradiation was performed for preset time. 30 min later, the cells were collected and resuspended in 1 mL JC-1 solution (2.5 μg mL^{-1}) for 30 min. The samples were washed twice with PBS and analyzed by Beckman Flow Cytometer.

In Vivo Antitumor Study: All animal experiments were performed according to the guidelines for laboratory animals established by the Wuhan University Center for Animal Center Experiment/A3-Lab. Mice were injected with 100 μL H22 cells. When the tumors reached an approximate size of 150 mm^3, the mice were divided into several groups randomly and each group was 4 mice. For intravenous injection, the mice were injected with 100 μL PBS buffer, $(KLAKLAK)_2$ and PPK at the 1st day and 6th day, respectively. And 20-min light irradiation was performed after injected for 24 h (630 nm, 220 mW cm^{-2}). For subcutaneous injection, the mice were injected with 100 μL PBS buffer, $(KLAKLAK)_2$, PpIX and PPK respectively. 2 h later, PPK group received 5-min light irradiation. After 4 h, the PPK and PpIX groups received 15 and 20 min light irradiation, respectively. The dose of PpIX was 5 mg kg^{-1} per mouse while $(KLAKLAK)_2$ was 13.2 mg kg^{-1} per mouse. The tumor size and mice weight were measured immediately before injection. The tumor volume was defined as: $V = ((\text{tumor length}) \times (\text{tumor width})^2)/2$. Relative tumor volume was defined as V/V_0 (V_0 was the tumor volume when the treatment was initiated), while the relative body weight was defined as M/M_0 (M_0 was the body weight of mouse when the treatment was initiated).[38] After the mice were sacrificed, the muscle, heart, liver, spleen, lung, kidney, and tumor tissue were collected. H&E staining was used for histological examinations.[39]

In Vivo Optical Imaging, Tissue Distributions, and Pharmacokinetics: H22 tumor-bearing mice were injected intravenously via tail vein with 100 μL PPK solution (22 mg kg^{-1} per mouse). Mice were anesthetized and imaged at the preset time after injection of PPK. The excitation wavelength was 630 nm, and long wave fluorescence emission (600–700 nm) was measured. To determine the tissue distribution, mice were sacrificed at the 24th h after injection of PPK. The tissues including muscle, heart, liver, spleen, lung, kidney, and the tumor were collected and imaged. For pharmacokinetic studies, mice were injected with PPK (22.15 mg kg^{-1} per mouse) via tail vein. The blood samples were taken at the 0.5, 1, 4, 8, 24, and 48 h time points after intravenous injection. Appropriate PBS was added and then the samples were repeatedly freeze-thawed. The samples were under ultrasound for 5 min and then centrifugated at 3000 r min^{-1} for 4 min. The supernate was measured by using fluorescence spectroscopy. The amount of PPK was obtained from standard curves determined by fluorescence spectrum (E_x = 409 and E_x = 630 nm).

Statistical Analysis: Statistical analysis was performed using a Student's t-test. The differences were considered to be statistical significant for p value <0.05.

Supporting Information

Supporting Information is available from the Wiley Online Library or from the author.

Acknowledgements

This work was financially supported by the National Natural Science Foundation of China (Grant Nos. 51125014, 51233003, and 21474077), the National Key Basic Research Program of China (Grant No. 2011CB606202), the Ministry of Education of China (Grant No. 20120141130003) and the Natural Science Foundation of Hubei Province of China (Grant No. 2013CFA003).

Received: February 11, 2015
Revised: March 13, 2015
Published online: April 8, 2015

[1] S. Mura, J. Nicolas, P. Couvreur, *Nat. Mater.* **2013**, *12*, 991.
[2] V. P. Torchilin, *Nat. Rev. Drug Discov.* **2014**, *13*, 813.
[3] R. Mo, T. Jiang, R. DiSanto, W. Tai, Z. Gu, *Nat. Commun.* **2014**, *5*, 3364.
[4] H. Wei, R. X. Zhuo, X. Z. Zhang, *Prog. Polym. Sci.* **2013**, *38*, 503.
[5] H. L. Sun, B. N. Guo, R. Cheng, F. H. Meng, H. Y. Liu, Z. Y. Zhong, *Biomaterials* **2009**, *30*, 6358.
[6] K. Han, Q. Lei, H. Z. Jia, S. B. Wang, W. N. Yin, S. X. Cheng, X. Z. Zhang, *Adv. Funct. Mater.* **2015**, *25*, 1248.
[7] J. E. Chung, S. Tan, S. J. Gao, N. Yongvongsoontorn, S. H. Kim, J. H. Lee, H. S. Choi, H. Yano, L. Zhuo, M. Kurisawa, J. Y. Ying, *Nature Nanotechnol.* **2014**, *9*, 907.
[8] T. M. Allen, P. R. Cullis, *Science* **2004**, *303*, 1818.
[9] H. M. Wang, Z. M. Yang, *Soft Matter* **2012**, *8*, 2344.
[10] Y. Y. Yuan, R. T. K. Kwok, R. Y. Zhang, B. Z. Tang, B. Liu, *Chem. Commun.* **2014**, *50*, 11465.
[11] P. Huang, D. L. Wang, Y. Su, W. Huang, Y. F. Zhou, D. X. Cui, X. Y. Zhu, D. Y. Yan, *J. Am. Chem. Soc.* **2014**, *136*, 11748.
[12] A. G. Cheetham, P. Zhang, Y. Lin, L. L. Lock, H. G. Cui, *J. Am. Chem. Soc.* **2013**, *135*, 2907.
[13] Z. Y. He, B. Y. Chu, X. W. Wei, J. Li, C. K. Edwards III, X. R. Song, Y. M. Xie, Y. Q. Wei, Z. Y. Qian, *Int. J. Pharm.* **2014**, *469*, 168.
[14] R. K. Pathak, S. Marrache, J. H. Choi, T. B. Berding, S. Dhar, *Angew. Chem.* **2014**, *126*, 1994.
[15] L. M. Pan, J. N. Liu, J. L. Shi, *Adv. Funct. Mater.* **2014**, *24*, 7318.
[16] Y. L. Li, L. Zhu, Z. Z. Liu, R. Cheng, F. H. Meng, J. H. Cui, S. J. Ji, Z. Y. Zhong, *Angew. Chem. Int. Ed.* **2009**, *48*, 9914.
[17] H. L. Tu, Y. S. Lin, H. Y. Lin, Y. Hung, L. W. Lo, Y. F. Chen, C. Y. Mou, *Adv. Mater.* **2009**, *21*, 172.
[18] J. F. Lovell, T. W. B. Liu, J. Chen, G. Zheng, *Chem. Rev.* **2010**, *110*, 2839.

[19] M. P. Gillmeister, M. J. Betenbaugh, P. S. Fishman, *Bioconjugate Chem.* **2011**, *22*, 556.
[20] C. S. Jin, L. Y. Cui, F. Wang, J. Chen, G. Zheng, *Adv. Healthcare Mater.* **2014**, *3*, 1240.
[21] C. A. Robertson, D. Hawkins Evans, H. Abrahamse, *J. Photochem. Photobiol., B: Biol.* **2009**, *96*, 1.
[22] V. Soto-Cerrato, E. Llagostera, B. Montaner, G. L. Scheffer, R. Perez-Tomas, *Biochem. Pharmacol.* **2004**, *68*, 1345.
[23] H. Y. Ding, B. D. Sumer, C. W. Kessinger, Y. Dong, G. Huang, D. A. Boothman, J. M. Gao, *J. Controlled Release* **2011**, *151*, 271.
[24] H. Cabral, Y. Matsumoto, K. Mizuno, Q. Chen, M. Murakami, M. Kimura, Y. Terada, M. R. Kano, K. Miyazono, M. Uesaka, N. Nishiyama, K. Kataoka, *Nat. Nanotechnol.* **2011**, *6*, 815.
[25] H. M. Ellerby, W. Arap, L. M. Ellerby, R. Kain, R. Andrusiak, G. D. Rio, S. Krajewski, C. R. Lombardo, R. Rao, E. Ruoslahti, D. E. Bredesen, R. Pasqualini, *Nat. Med.* **1999**, *5*, 1032.
[26] H. Park, K. Na, *Biomaterials* **2013**, *34*, 6992.
[27] K. S. Kim, W. Park, K. Na, *Biomaterials* **2015**, *36*, 90.
[28] L. Dong, Y. Liu, Y. Lu, L. Zhang, N. Man, L. Cao, K. Ma, D. An, J. Lin, Y. Xu, W. P. Xu, W. B. Wu, S. H. Yu, L. P. Wen, *Adv. Funct. Mater.* **2013**, *23*, 5930.
[29] X. C. Ma, X. B. Wang, M. Zhou, H. Fei, *Adv. Healthcare Mater.* **2013**, *2*, 1638.
[30] L. Agemy, D. Friedmann-Morvinski, V. R. Kotamraju, L. Roth, K. N. Sugahara, O. M. Girard, R. F. Mattrey, I. M. Verma, E. P. Ruoslahti, *P. Natl. Acad. Sci. USA.* **2011**, *108*, 17450.
[31] N. Larsona, J. Y. Yang, A. Ray, D. L. Cheney, H. Ghandehari, J. Kope ek, *Int. J. Pharm.* **2013**, *454*, 435.
[32] H. C. Tsai, T. Imae, G. Calderó, C. Solans, *J. Biomed. Mater. Res. A* **2012**, *100A*, 746.
[33] D. Kedracki, P. Maroni, H. Schlaad, C. Vebert-Nardin, *Adv. Funct. Mater.* **2014**, *24*, 1133.
[34] N. Hardy, H. M. Viola, V. P. A. Johnstone, T. D. Clemons, H. C. Szappanos, R. Singh, N. M. Smith, S. K. Iyer, L. C. Hool, *ACS Nano* **2014**, *9*, 279.
[35] K. Han, S. Chen, W. H. Chen, Q. Lei, Y. Liu, R. X. Zhuo, X. Z. Zhang, *Biomaterials* **2013**, *34*, 4680.
[36] K. Han, Y. Liu, W. N. Yin, S. B. Wang, Q. Xu, R. X. Zhuo, X. Z. Zhang, *Adv. Healthcare Mater.* **2014**, *3*, 1765.
[37] A. Sahu, W. I. Choi, J. H. Lee, G. Tae, *Biomaterials* **2013**, *34*, 6239.
[38] H. H. Bu, X. Y. He, Z. W. Zhang, Q. Yin, H. J. Yu, Y. P. Li, *Int. J. Pharm.* **2014**, *471*, 206.
[39] J. Silva-Correia, B. Zavan, V. Vindigni, T. H. Silva, J. M. Oliveira, G. Abatangelo, R. L. Reis, *Adv. Healthcare Mater.* **2013**, *2*, 568.